Computer detection of the rapid diffusion of fluorescent membrane fusion markers in images observed with video microscopy

Walter D. Niles,* Qing Li, and Fredric S. Cohen
Department of Physiology, Rush University, Chicago, Illinois 60612 USA

ABSTRACT We have developed an algorithm for automated detection of the dynamic pattern characterizing flashes of fluorescence in video images of membrane fusion. The algorithm detects the spatially localized, transient increases and decreases in brightness that result from the dequenching of fluorescent dye in phospholipid vesicles or lipid-enveloped virions fusing with a planar membrane. The flash is identified in video images by its nonzero time derivative and the symmetry of its spatial profile. Differentiation is implemented by forward and backward subtractions of video frames. The algorithm groups spatially connected pixels brighter than a user-specified threshold into distinct objects in forward- and backward-differentiated images. Objects are classified as either flashes or noise particles by comparing the symmetries of matched forward and backward difference profiles and then by tracking each profile in successive difference images. The number of flashes identified depends on the brightness threshold, the size of the convolution kernel used to filter the image, and the time difference between the subtracted video frames. When these parameters are changed so that the algorithm identifies an increasing percentage of the flashes recognized by eye, an increasing number of noise objects are mistakenly identified as flashes. These mistaken flashes can be eliminated by a human observer. The algorithm considerably shortens the time needed to analyze video data. Tested extensively with phospholipid vesicle and virion fusion with planar membranes, our implementation of the algorithm accurately determined the rate of fusion of influenza virions labeled with the lipophilic dye octadecylrhodamine (R18).

INTRODUCTION

Diffusion of fluorescent probes has long been used to study fusion between membranes (Frye and Edidin, 1970). The release or mixing of water-soluble and membrane-bound dye probes from individual fusing membranes or their enclosures is increasingly being followed by video fluorescence microscopy. Concentration quenching of a dye's fluorescence occurs when the probe is packed into a particle at a high density. Upon membrane fusion, diffusion of the dye away from the release site decreases its concentration and relieves the self-quenching of fluorescence. Thus, the brightness of a small, spatially localized region in the video image initially increases. Later, as the dye continues to spread after relief of the quenching, the diameter of the bright area grows, yet its intensity diminishes. This "flash" follows a characteristic spatiotemporal profile of brightness that is readily detected by eye in video microscope images of vesicle or virion fusion with planar membranes (Niles and Cohen, 1987; Woodbury and Hall, 1988; Perin and MacDonald, 1989; Niles and Cohen, 1991*a*) and virion fusion with erythrocytes (Lowy et al., 1990). Detecting flashes can be used to estimate fusion rates (Niles and Cohen, 1991*a, b*). In addition, brightness profiles can be used to study both diffusion and fluorescence dequenching of the probe (Niles and Cohen, 1987; Chen and Blumenthal, 1989; Rubin and Chen, 1990; Lowy et al., 1990; Georgiou et al., 1989) and to detect erythrocyte fusion with cells (Sarkar et al., 1989). Similarly, the spread of fluorescent markers, initially contained in a subset of red cell membranes, can be tracked using video microscopy to study polyethylene glycol-induced fusion (Huang et al., 1990, Huang and Hui, 1990).

The quantity of video information in the flashes is overwhelming, as the spatial profile changes on a time scale longer than the video sampling rate of 30 frames/s (Niles and Cohen, 1987). Flashes may occur at a high rate with several appearing at the same time. This makes nonautomated analysis of the data impossible even with the most tedious effort. A computer automated detector must be able to track flashes varying in duration, maximum area, and brightness even within a single experiment. It must also recognize flashes that are obscured by spatial variation of the background fluorescence because of dye released by previous fusion events and the presence of nonfusing fluorescent objects. The rapidly changing brightnesses must be extracted from a potentially noisy background within a reasonable computational time.

We have semiautomated flash analysis by developing a computer algorithm that detects flashes in video images of vesicle or virion fusion with planar membranes. The algorithm differs from a prior flash detection procedure (Woodbury, 1986) in that it relies on region processing of the time-differentiated image rather than point processing of the raw image. Region processing allowed a strategy based on group classification of objects to identify flashes (Toussaint, 1980; Lenz, 1989). Our algorithm was implemented with an image processor rather than a host computer to perform the computations. This yielded a speedup of ~500 compared with the previous procedure, thereby making automated detection feasible as an analytical tool. We have tested the algorithm with a wide variety of video scenes of mem-

* Address correspondence to Walter D. Niles.

0006-3495/92/09/710/13 $2.00

brane fusion, including those with high levels of background noise, and used it to measure the fusion rate of influenza virions, labeled with the lipophilic fluorescent probe R18, with planar membranes. The pattern recognition program accurately detects flashes if user-specified detection criteria are optimally set.

MATERIALS AND METHODS

Phospholipid vesicles and influenza virions were labeled with calcein and R18, respectively, according to published procedures (Niles and Cohen, 1987, 1991*a*). Video microscopy of vesicle and virion fusion with planar lipid membranes were performed using a specially modified fluorescence microscope and planar bilayer chamber as previously described in detail (Niles and Cohen, 1987, 1991*a*). Fluorescently labeled vesicles or virions were delivered to the planar membrane, maintained at conditions favorable for fusion, by pressure-ejection from a pipette. The ensuing flashes were viewed through the microscope with a video camera.

Video microscope

A flash was detected by its temporally changing spatial distribution of brightness. The ability to detect changes in the brightness distribution was limited by the spatial resolution of the video microscope system. Resolution was determined by both the diffraction-limited resolution of the objective lens of the microscope and the horizontal resolution of the video cameras and recording equipment. The objectives had long working distances and low numerical aperture (20× MPlan, N.A. 0.4; Nikon Inc., Melville, NY, or a Plan 25×, N.A. 0.4 infinity-corrected; E. Leitz Inc., Rockleigh, NJ); the diffraction-limited optical resolution was ~750 nm. We used either a silicon intensified target camera (model SIT 66; Dage-MTI, Inc., Michigan City, IN) or an image intensifier (model KS-1381; Video Scope International, Washington, DC) in tandem with a charge-coupled device camera (model CCD 72×, Dage-MTI, Inc.). Both cameras produced monochrome video signals conforming to the NTSC/RS170-330 standard with a 525 line, 2:1 interlaced frame at a rate of 30 Hz. Fainter flashes were detected with the intensified CCD camera because of its greater sensitivity (2 μlux), and the edges of flash profiles were more distinct because of its greater horizontal resolution (650 lines). Background noise at low light levels made flash outlines irregular and jagged in the video image. The SIT camera had lower background noise, but its lesser sensitivity, longer persistence, and luminance-dependent horizontal resolution (100 lines at 10 μlux increasing to 550 lines at 100 μlux) distorted the brightness profiles. These effects were apparent on the video monitors (model ECM 1301 or EVM1719; Electrohome, Ltd., Kitchener, Ontario, Canada), which had a reduced scan full-frame width of 315 mm, representing 225 μm in the specimen plane.

Video signals from both cameras were stored on U-matic tape using a high horizontal resolution (>400 lines) monochrome tape recorder (model VO 5800H; Sony Communications Corp., Parsippany, NJ). To ensure accurate frame registration in digitization, the video records selected for analysis were transferred to a high-resolution (530 lines) monochrome optical disk (model TQ 3038F; Panasonic Corp., Secaucus, NJ). Line jitter in the tape signal (Inoue, 1986) was decreased to <15 ns with a 14.3 MHz sampling rate time-base corrector (Sync 2F; Nova Systems Inc., Canton, CT) interposed between the tape and disk recorders.

Image processor

The image processor (series 151; Imaging Technology Inc., Bedford, MA) was controlled by a 25 MHz AT-class host microcomputer (Addonics 386; Addonics, Inc., Taipei, Taiwan) with custom software written in C (version 5.1; Microsoft Corp., Redmond, WA). This particular processor used a partial (24-bit address) VME standard backplane as a video bus. The host microcomputer was connected to the bus via a 20 bit-to-24 bit address translator. The bus connected together application modules of the image processor, including the analogue-to-digital converter, eight frame buffers, and other computational modules.

Video frames containing flashes were digitized at 512 pixels/line, 8-bit brightness resolution/pixel after being fed frame-by-frame from the optical disk to the A/D converter (10 MHz sampling rate) under host computer control. For each frame, the 480 lines containing video information were stored in a frame buffer with the even and odd fields of the video frame interlaced to enable filtering of the frame by spatial convolution. The digitization frequency of 512 pixels/line was greater than the spatial resolution limits imposed by the video microscope (0.75 μm), as each pixel covered a distance corresponding to ~0.44 μm in the specimen plane.

Preprocessing relied on three computational modules connected to the video bus: an arithmetic logic unit, a real-time convolution unit (RTC), and a histogram-feature extraction unit (HF). The arithmetic logic unit performed arithmetic and logical operations with 16-bit integer precision, including the pixel-by-pixel subtraction of two video frames used to obtain difference images. Brightness differences were represented as 8-bit integers. The RTC, with four parallel digital signal processors, performed spatial convolution and other filtering operations. The HF module stored the histogram of brightness values in a single video frame but could be programmed to be a "streak" detector. A streak is a sequence of contiguous pixels on a single video line whose brightness equals or exceeds a user-set threshold value. In streak detection mode, the HF unit stored the leftmost starting location (pixel number) and the length count in pixels of each streak on each video line. The resulting output array of streaks was read by the host computer for analysis. Frame computations and storage were synchronized with the video rate of 30 Hz.

Flash detection algorithm

Basic strategy of the method

Since the flash was a spatially localized, dynamically changing area of brightness, our algorithm relied on general principles of dynamic pattern recognition (Martin and Aggarwal, 1979; Castleman, 1979; Ballard and Brown, 1982; Yalamanchili et al., 1982). We identified and analyzed only those regions of the video image that changed over time. In our experiments, time-varying profiles originated from both the desired flashes and unwanted fluorescent particles that moved by the stirring of the buffer-filled compartment bathing the planar membrane and the velocity field of pipette ejections of fluorescent vesicles or virions. The origins of these profiles were distinguished on the basis that, ideally, a flash spread out symmetrically from a stationary point, whereas a laterally moving particle had an invariant brightness profile that was asymmetric in a difference image due to the motion of its centroid.

The algorithm is outlined in Fig. 1. First, the areas that changed with time were isolated by temporal differentiation. This was performed by subtracting sequential video frames to produce difference images. Noise was reduced by spatial filtering of each difference image. Then the shapes of bright areas in each difference image were analyzed. As seen in the sequence of frames of a vesicle flash shown in Fig. 2 *A*, flash profiles were only roughly circular in shape. Although profiles of flashes in difference images were annular as expected for diffusion profile differences (Fig. 2 *B*), these shapes were often very irregular (Fig. 2 *B*; see also Fig. 6 *B*). Therefore, comparing changes in the brightness distributions with stored templates of predetermined shapes (e.g., circles or annuli) as used in traditional pattern recognition methods (Kimme et al., 1975; Ballard and Brown, 1982; Illingworth and Kittler, 1988) was not feasible. To analyze the profiles, we used a more general classification scheme. Spatially connected bright pixels in the difference image were grouped into distinct objects (Toussaint, 1980; Lenz, 1989). To maintain temporal resolution, objects were identified separately in the even and odd fields of each frame. Objects were classified as either flashes or moving particles by analyzing the symmetry of their

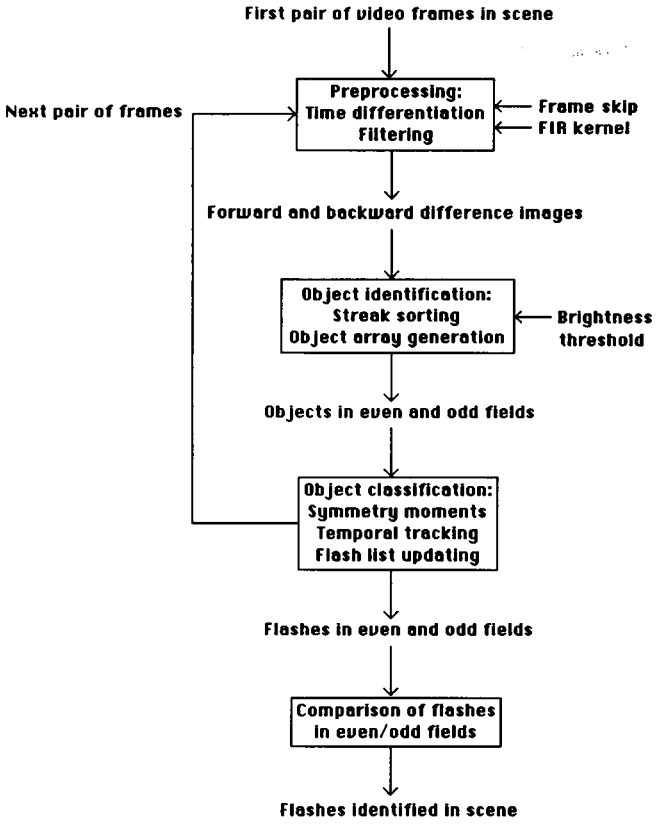

FIGURE 1 Outline of flash detection algorithm. The frame skip or delay, FIR kernel size and brightness threshold were set in the image processor and host computer before processing a scene. Sequential pairs of frames were subtracted (time-differentiated) and filtered in two sequential convolution operations. Streaks were detected and sorted into objects. Streaks on even and odd lines of the difference image were sorted separately, and the objects were stored in separate arrays, one for each video field. To assess movement, objects in the forward and backward difference images (obtained by reversing the order of subtraction of the frame pair used in forward differentiation) were matched by comparing their centroid positions and the symmetry of their spatial brightness distributions. The algorithm then processed the next two video frames in the scene. The objects identified in this difference image were compared with the flashes identified in the prior image to track flashes temporally. At the end of a scene, the flashes identified in the even and odd fields were correlated into a single list.

shapes and the movement of their centroids, and then by tracking the objects between successive difference images. Objects were tracked by matching the spatial positions of objects in two difference images and then by comparing their brightness distributions. Finally, the flashes in the even and odd fields were compared and matched, yielding a list containing the properties of all flashes identified in a scene. Because numerous issues were encountered in developing automated flash detection, salient specific details of the algorithm and critical features of its implementation are discussed for each of these steps.

Temporal differentiation

For each pair of video frames, the forward difference image was calculated by subtracting the pixel brightness of the earlier frame from their corresponding values in the later frame. Negative brightnesses were set to zero. In Fig. 2 *A*, the second and third panels are the even and odd fields of the first frame of the vesicle flash. The second video frame of this flash is shown in the fourth panel. The two fields of the first frame were interlaced and then subtracted from the second frame to produce the forward difference image shown in the left panel of Fig. 2 *B*. The backward difference image (used in motion detection) was computed by subtracting the later frame from the earlier frame. The backward difference image corresponding to the left panel of Fig. 2 *B* is shown in the left panel of Fig. 2 *C*.

Flashes due to aqueous dye release from vesicles changed rapidly in intensity, because the water-soluble dye diffused quickly in the aqueous medium (Niles and Cohen, 1987). Thus, differences were large when subtracting two successive video frames (Fig. 2 *B*). With flashes arising from virion envelope fusion, however, the released lipophilic probe diffused slowly within the hydrocarbon milieu of the planar membrane, and the spatial distribution of brightness changed little over the 33-ms period between two successive video frames (Niles and Cohen, 1991*a*). To detect these flashes, rather than subtracting successive video frames, either every other frame was subtracted (referred to as a "skip" or "delay" of 1 frame) or every first frame in a sequence was subtracted from every fourth frame (a skip of 2 frames). With nonzero skips, the intervening frames were not processed. These frame skips of zero, one, and two were implemented as a user-specified parameter to make the algorithm useful for both types of flashes.

Noise reduction and edge enhancement

The difference images contained not only flashes and moving particles, but also video and fluorescence noise originating from camera fluctuations and nonuniformities in the fluorescence background. Background noise could cause a single flash to appear as several small objects in the difference image. Noise was decreased by filtering each difference image in two spatial convolution operations. These operations replaced the brightness $b(x, y)$ of each pixel with the locally weighted average brightness of the adjacent pixels, which formed an i-column, j-row matrix $\{b(x, y)_{ij}\}$. The weights were elements of a kernel matrix, $\{a_{ij}\}$; the new pixel brightness was equal to the scalar product $\{a_{ij}\} \cdot \{b(x, y)_{ij}\}$.

A 4×4 square-matrix convolution kernel, shown below, sharpened vertical edges and reduced brightnesses of isolated pixels. The kernel was

$$\begin{bmatrix} 0 & 1 & 1 & 0 \\ 0 & 1 & 1 & 0 \\ 0 & 1 & 1 & 0 \\ 0 & 1 & 1 & 0 \end{bmatrix}$$

and, with the columns and rows numbered 1 through 4, top to bottom and left to right, the argument pixel was located at position $(i, j) = (2, 2)$.

Then, horizontal edges were sharpened with a 16×1 row-matrix kernel. The new brightness value for each pixel was the weighted average of the 16 contiguous pixels to the right and left of the test pixel (8 on each side), and the operation was implemented with the finite-impulse response (FIR) filtering mode of the RTC. The kernel was a user-specified parameter, because flashes came in a great variety of sizes, and this filtering increased the intensities of profiles having widths similar to the nonzero part of the kernel. For larger flashes, the 16 kernel elements consisted of all 1s. For smaller flashes, the eight center elements were 1s and the first and last four elements were 0s. The difference profiles in the right panels of Fig. 2, *B* and *C* are the images of the respective left panels after convolution with first the 4×4 kernel and then the small, eight nonzero element FIR kernel.

Object recognition

Streak generation. After subtraction and filtering, the bright pixels in the difference image were grouped into objects. We defined an object as a two-dimensional spatial profile corresponding to a contiguous fluorescent region in a difference image. Objects were constructed from spatially connected streaks. Streaks were identified by the streak detector as contiguous pixels in the same video line with intensities at least that of the threshold value (see Materials and Methods). Because flashes exhibited a wide intensity range, the threshold was user selectable.

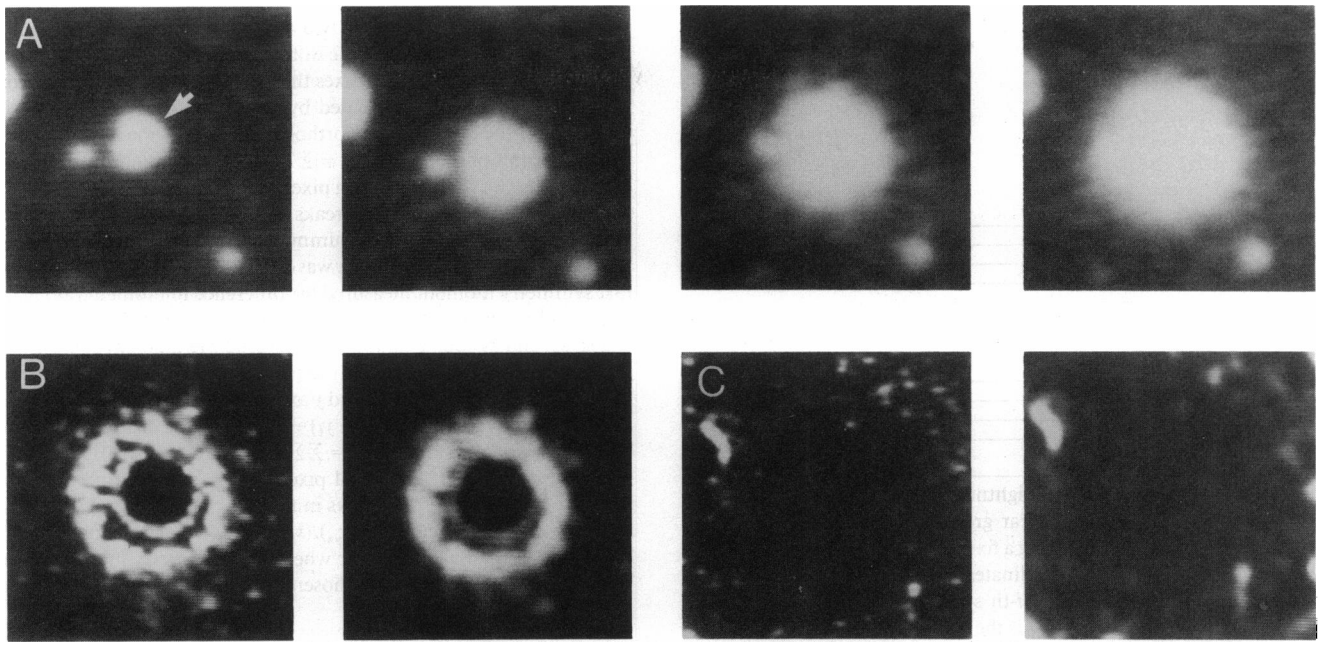

FIGURE 2 A sequence of video frames of a single vesicle flash. (*A*) Unprocessed sequential video images. The first panel shows a small region of the video frame immediately before the flash, with the vesicle marked by an arrow. The second panel shows the even (earlier) field of the next video frame, just after the eruption of the flash. The third panel shows the odd (later) field of the same frame. The flash profile changed in diameter during the intervening 16.7 ms. The fourth panel shows the next (second) frame of the flash with the two fields interlaced. The variegation of the profile due to the interlacing of the two spatial profiles sampled 1/60 s apart is apparent. (*B*) The forward difference image produced by interlacing the fields shown in the second and third panels in *A* and subtracting this frame from the second frame (fourth panel in *A*) is shown in the left panel. The profile is annular in shape, as expected for the temporal difference of diffusion profiles. The right panel shows the difference image after two convolution operations, first with the 4×4 square-matrix kernel and then with the small 8-nonzero element 16×1 row-matrix FIR kernel. (*C*) The backward difference image produced by reversing the order of the frames used in the subtraction, before (left) and after (right) convolution as in *B*. The flash profile is greater in intensity as well as area in the later frame, because of the dequenching of the dye fluorescence, and the subtraction leaves a dark profile. The field width of each panel is ~ 12 μm.

Thresholds of 20, 40, or 60 brightness units on a scale of 0 to 255 proved to cover the range needed to accurately identify flashes.

The luminance data in each RS170/330-format video frame consisted of two interlaced fields of 240 lines each, with each location in the image sampled twice separated by a period of 1/60 s. As the flash spatial profiles changed during the scanning of the entire video frame (1/30 s), streaks were grouped into objects separately for each of the two fields according to the line number of the streak. If a flash erupted during the scan of the odd (later) field, the flash image would be interlaced with blank lines from the even (earlier) field and produce a vertically variegated image in the full video frame. Maintaining two sets of objects, one for each field, until collation into a single list after processing all frames in a scene avoided this loss of temporal resolution.

Data structures. Grouping streaks into objects within a single difference image and tracking the objects in multiple frames were implemented with two types of arrays. The first type, the object array, was a list of all objects—those in the currently processed image as well as all the flashes encountered in prior frames. The second type, the active array, contained the subset of these objects or flashes that were "active": they were either being generated or tracked and could be modified by the processing. During the generation of objects for a single difference image, the object array contained pointers to each object's constituent streaks. The active array consisted of pointers to the incomplete objects to which streaks still could be added.

A flash was a set of objects with different spatial profiles that occurred at the same spatial location in several successive difference images. To organize the different objects comprising each flash, we used the object array as a flash list. Objects identified in the current difference image were matched with unexpired flashes from the previous image. Pointers to these unexpired flashes were placed in an active flash array and coordinated the matching. These data structures enabled the correlation of objects generated within a single video frame with objects in prior frames to build flashes.

Sorting streaks into objects. Objects were constructed in each difference image from spatially adjacent streaks. Each streak was compared with objects already in the list, and if it was not spatially contiguous with an extant object, a new object was created. Contiguous streaks were grouped into objects by sorting the streaks in order from the top left of the video frame to the bottom right. The sorting procedure was implemented as follows, with each streak denoted as an ordered triple (x_i, y_i, l_i), where x_i is the pixel number and y_i is the line number of the leftmost pixel in the streak, and l_i is the length of the streak in pixels. The vertical positions of the streaks were first compared. If the current streak with line number y_i was separated from the last streak processed (with line number y_{i-1}) by at least two video lines ($y_i > y_{i-1} + 2$), then it was assigned to a new, active object. If the current streak lay on either the same video line as the last streak processed or on the next line down ($y_i = y_{i-1}$ or $y_i = y_{i-1} + 2$), its horizontal position was compared with all the active objects. For the current streak (x_i, y_i, l_i) to be vertically contiguous with a streak in an active object, (x_j, y_j, l_j), where $y_j = y_i - 2$, at least one of the following conditions had to be satisfied:

$$x_i \geq x_j \quad \text{and} \quad x_i \leq x_j + l_j, \tag{1}$$

$$x_i + l_i \geq x_j \quad \text{and} \quad x_i + l_i \leq x_j + l_j, \tag{2}$$

$$x_i \leq x_j \quad \text{and} \quad x_i + l_i \geq x_j + l_j, \quad \text{or} \tag{3}$$

$$x_i \geq x_j \quad \text{and} \quad x_i + l_i \leq x_j + l_j. \tag{4}$$

When vertical overlap with an active object occurred, the streak was assigned to that object; multiple active objects connected by a single

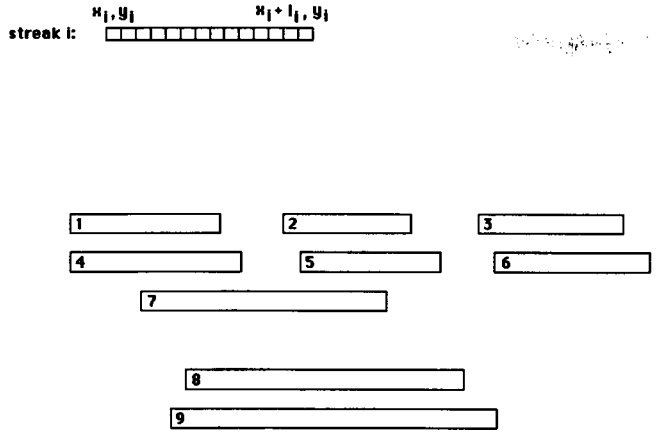

FIGURE 3 Sample streaks of a brightness profile. The schematic shows several hypothetical streaks: linear groups of contiguous pixels with brightnesses equal to or exceeding a fixed threshold. The top part of the figure diagrams the streak coordinates referred to the pixel and line numbering of a frame. For the i-th streak, the leftmost pixel in the streak is denoted (x_i, y_i), where x_i is the pixel number and y_i is the video line number, and the rightmost pixel is $(x_i + l_i, y_i)$, where l_i is the length of the streak in pixels. In the lower part, nine hypothetical streaks are placed as they might be in a difference image. For simplicity, we show only the streaks from a single video field; the lines from the other field are left as gaps. The contiguous streaks were grouped into the objects as described in the text.

streak were joined. If overlap did not occur, the streak created a new object. Sorting continued with the next streak.

In Fig. 3, we illustrate nine streaks from a hypothetical difference image. These streaks would be processed into three distinct objects as follows. The three individual streaks on the first line would be initially assigned to three newly created, active objects: O_1, O_2, and O_3. On the second line, streak 4, contiguous with streak 1, would be assigned to O_1; streak 5, contiguous with streak 2, would be assigned to O_2; and streak 6, contiguous with streak 3, would be assigned to O_3. On the third line, streak 7 connects O_1 and O_2. The algorithm would join O_2 to O_1 and create a new O_1 containing streaks 1, 2, 4, 5, and 7 and would rename O_3 to O_2. Streaks 8 and 9 would subsequently generate a new O_3. Joining thus resulted in grouping initially separate objects into a single object, allowing single objects with spatial brightness profiles that were not convex but highly variegated in shape to be recognized. Current streaks were added only to active objects. When no streaks were adjacent to an active object, the object was "closed" by removing its pointer from the active array. Two object arrays were generated for each video frame, one for each video field, by sorting the streak table twice. The starting line number was offset by 1 to shift between even and odd lines.

Object classification into flashes

Object data (moments). Objects were initially classified into flashes and noise objects (e.g., moving particles) by analyzing their spatial brightness profiles. Each object was characterized by its center-of-brightness point (centroid), the spatial distributions of brightness around the centroid along orthogonal axes (symmetry), the number of the video frame in which it was first detected, and the number of frames in which it was tracked. The centroid of each object was defined as the average x- and y-positions of its streaks, which is the (1, 1) central moment (Castleman, 1979). The average x-position, x_j, for O_j was calculated by weighting the x-position at the center of each streak, $x_i + l_i/2$ by the number of pixels in the streak, l_i: $x_j = [\Sigma\ (2x_i + l_i)l_i/2]/\Sigma\ l_i$, where the summation was over the streaks in the object. The average y-position (video line number), y_j, was calculated as $\Sigma\ y_i l_i/\Sigma\ l_i$.

The brightness distribution of a flash in a difference image was expected to be spatially symmetric around the centroid. The symmetry of each object was quantified with two multidimensional moments (Castleman, 1979) that measured the difference between the spatial distributions along two orthogonal axes through the centroid. The distribution along an axis was computed by summing the distance between each pixel of the object and the orthogonal axis. For the moment along the y-direction of object O_j, $s_{yy} = \Sigma\ l_i|y_i - y_j|$, where (x_j, y_j) was the centroid, (x_i, y_i) was the starting pixel of each streak in the object, and the summation was over the streaks in O_j. For the x-direction, $s_{xx} = \Sigma\Sigma\ |x_i - x_j|$, where the inner summation was over all pixels within a streak and the outer summation was over all streaks in the object. The first symmetry moment measured the difference in moments along the x- and y-directions and was set equal to $(s_{yy} - s_{xx})/(s_{yy} + s_{xx})$.

The second symmetry moment measured the difference of the spatial distribution with respect to the pair of orthogonal xy and yx axes located at a 45° angle to the x and y axes. The distribution across the xy axis, s_{xy}, was given by $\Sigma\Sigma\ |(x_i + y_i) - (x_j + y_j)|$; the distribution across the yx axis was measured as $s_{yx} = \Sigma\Sigma\ |(x_i - y_i) - (x_j - y_j)|$, where the inner summations were over all pixels within a streak and the outer summations were over all streaks in the object. The second symmetry moment was set equal to $(s_{xy} - s_{yx})/(s_{xy} + s_{yx})$. An object's spatial distribution was scored as symmetric when both symmetry moments were <0.4, which was arbitrarily chosen to maximize the detection of flashes.

Flashes vs. moving objects. The lateral movement of fluorescent particles along the plane of the membrane was an important source of objects that did not originate from flashes. These objects were distinguished on the basis that flashes were expected to have stationary centroids and symmetric profiles, whereas moving objects were expected to have varying centroids and asymmetric profiles in difference images. This discrimination was accomplished by matching objects in forward and backward difference images where the backward difference image was computed by subtracting the later frame from the earlier frame. The distances between the positions of the centroids of the forward (x_f, y_f) and backward objects (x_b, y_b) were calculated as $\sqrt{[(x_f - x_b)^2 + (y_f - y_b)^2]}$. Forward and backward objects lying within a 40-pixel distance were matched, and the components of their symmetry moments were compared. Unmatched symmetric forward objects and those matched with at least one symmetric backward neighbor with a different spatial distribution were maintained in the forward object array as possible flashes. Both symmetric and asymmetric forward objects matched with backward objects having identical spatial distributions were identified as moving objects and deleted. Because some moving objects could be incorrectly scored as flashes by comparing only forward and backward difference images obtained from the same pair of frames, we also tracked the objects between sequential difference images.

Grouping objects into flashes by frame-to-frame tracking

The objects in the current difference image were matched with the active flashes (those identified in the immediately prior image) to determine whether the current objects were continuations of already extant flashes or were new flashes appearing in the image. Each object was paired with the nearest flash by pairing centroids lying within a distance of 40 pixels. If a match was found, the spatial profile of the object was compared with the profile of the flash (according to criteria previously described); if the profiles were different, the object was considered to be a continuation of the previously identified flash into the current difference image. If the spatial profiles of the object and the matched flash were the same, they were identified as a moving object and deleted from the list. The active flashes remaining without corresponding objects were closed by removing their pointers from the active flash array. The objects in the current difference image remaining unmatched were considered to be new flash events and entered into the flash list. The flash list was continually updated with newly identified flashes while keeping track of already identified and currently followed flashes.

After processing each difference image, the flash lists for the even and odd fields were compared to check that the same flashes were being

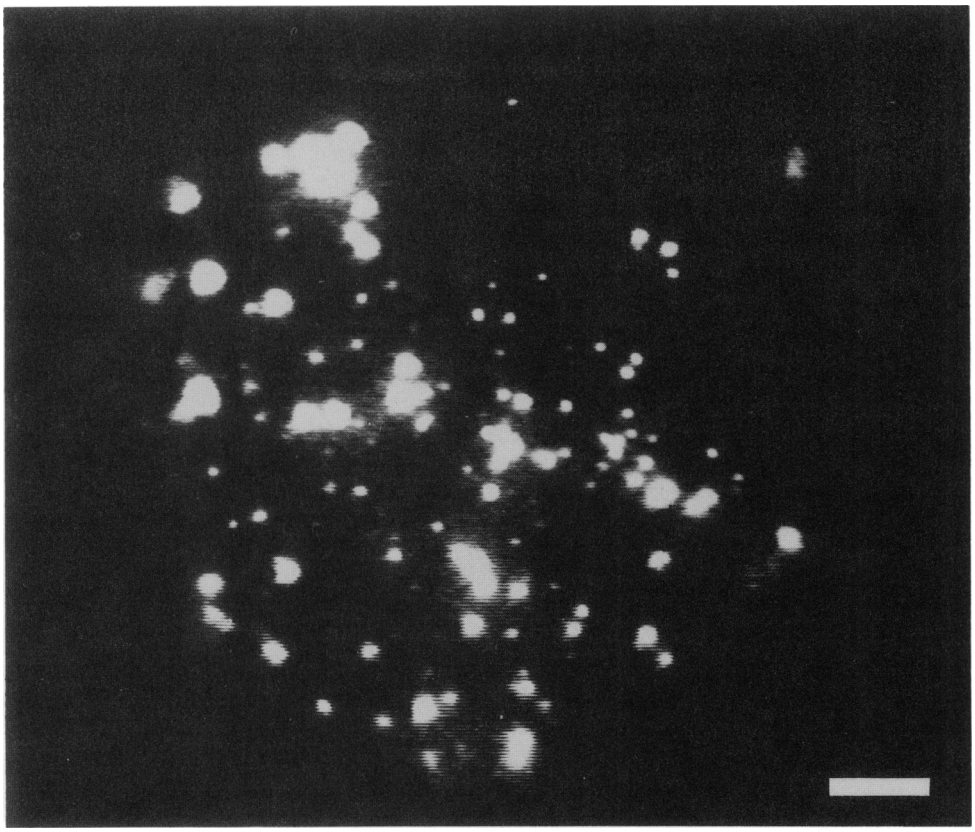

FIGURE 4 A single video frame from a vesicle flash scene. The planar membrane is viewed along its normal axis, and the frame was recorded with the SIT camera. The bright objects are fluorescent dye-filled vesicles bound to the planar membrane with calcium. The algorithm had to distinguish the lateral movements of unfused vesicles from the transient change in spatial profile characterizing dye release from a fused vesicle. The algorithm was 100% accurate in detecting vesicle flashes. Scale bar, 20 μm.

tracked. Flashes that were spatially and temporally overlapping were classed as the same flash and maintained on the flash list. At the end of processing a sequence of video frames, only those flashes detected in both even and odd fields were considered to be flashes. After the scene was processed, the two flash lists were displayed on a terminal as a single list and the centroids of the flashes were overlayed on the displayed image of the first video frame of the sequence.

RESULTS AND DISCUSSION

Our implementation of the algorithm was tested with a wide variety of scenes encountered when fluorescently labeled phospholipid vesicles and virions fused with planar membranes. With phospholipid vesicles, millimolar levels of calcium were used to establish vesicle adhesion with the planar membrane, and an osmotic gradient was used to promote vesicular swelling (Zimmerberg et al., 1980; Cohen et al., 1980; Niles and Cohen, 1987). With influenza virions, fusion was promoted by including gangliosides in the planar membrane to serve as virion receptors, holding the bath pH at ~5 and maintaining the temperature at 37°C (Niles and Cohen, 1991*b*). Although the fusion events were characterized by flashes in both systems, their video images were different. Adherent vesicles were very bright against the dark background of the membrane (Figs. 2, *A* and 4) and, due to stirring, their slow movement provided a large number of moving noise objects. Each flash originated from one of these vesicles. Virus preparations contained bright aggregates that did not bind to the membrane but were moved rapidly in the field of view by the stirring (Fig. 5). These aggregates did not produce flashes. The virus flashes originated de novo on a relatively bright fluorescence background. Furthermore, virus flashes were more variable in size and intensity. We tested the performance of the algorithm in these varied situations, particularly its ability to resolve flashes from bright, moving objects and to detect the less bright virion flashes against a noisy background. We explored the range of input parameters required to accurately detect each flash in any specific situation. In all situations, the algorithm processed each pair of frames in ~600 ms.

Performance of the algorithm was evaluated by comparing its detected flashes with those observed by eye in the same scene. Each scene began with an ejection of vesicles or virions toward the planar membrane and lasted for as long as flashes occurred, from 1 to 60 s. We defined the number of flashes recorded by the human observer in any scene as the "true" number of flashes, N_T, and the number of events detected by the algorithm as N_D. The number of true flashes accurately detected by

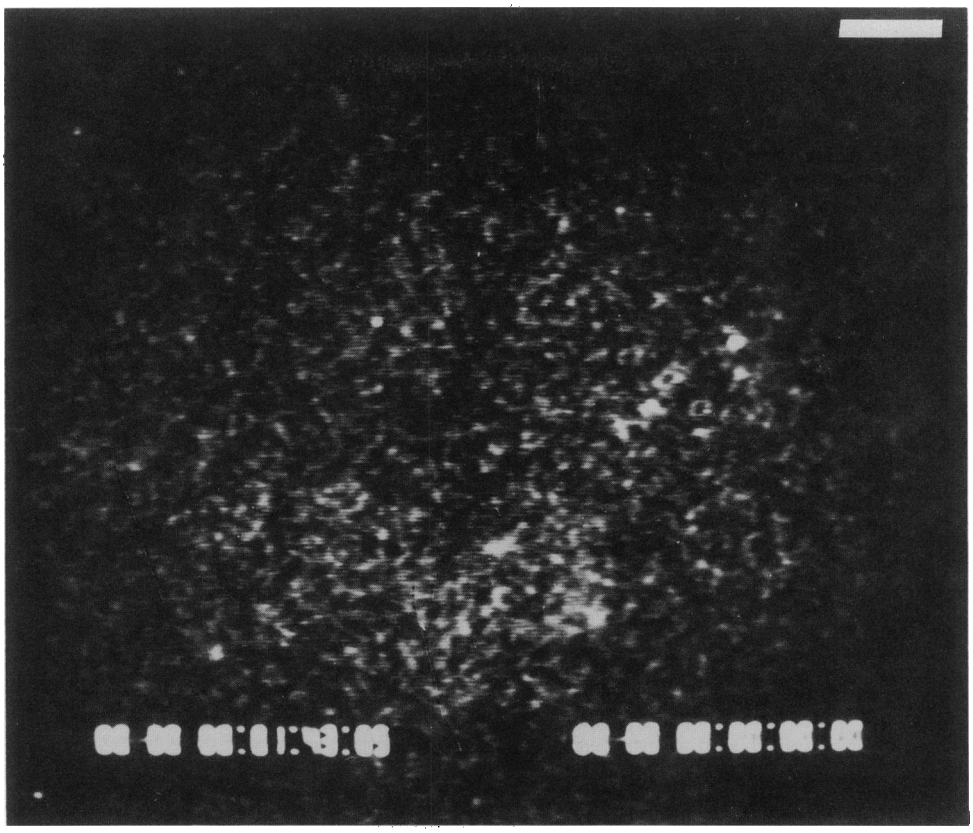

FIGURE 5 A single video frame from a virus flash scene. The planar membrane was viewed with an intensified CCD camera at 20% of maximum intensifier gain. Influenza virions labeled with R18 were ejected at the planar membrane from a pipette before recording this frame. The background was bright and noisy due to the amplified fluorescence of the diffuse ejecta and the bright aggregated material. These bright objects did not produce flashes but moved in the convection currents of the stirred bathing solution and sometimes became trapped in oscillatory eddies near the planar membrane. Flashes due to virion fusion with the planar membrane originated de novo on this bright background. The algorithm was less accurate in detecting these flashes. Scale bar, 20 μm.

the algorithm was denoted as N_A. We characterized the ability of the algorithm to identify (i.e., not miss) true flashes in a scene as the accuracy = N_A/N_T, which ranged from 0 to 1 but was undefined when flashes were not actually present in a scene. Not all detected events were assumed to be flashes, so we defined the specificity of detection as N_A/N_D. Specificity also ran from 0 to 1 and was undefined when no events were detected. These indices of performance were determined as a function of the input parameter settings for each scene.

Detection of phospholipid vesicle flashes

The algorithm detected the release of aqueous fluorescent dye from the phospholipid vesicles with an accuracy of 1. This originated from the clarity of the video scenes before, during, and after dye release. As seen in Fig. 4, the large labeled vesicles were very bright against the very low fluorescence background of the planar membrane and its bathing buffer. The fluorescence background remained low after a flash because the released dye diffused into an effectively infinite volume. The algorithm easily detected the changes in spatial brightness distribution of the bright dye released from the vesicles (Fig. 2 *B*). This was because diffusion of released dye in the aqueous medium was relatively fast, ~20 μm in 1/30 s. We tested 11 scenes of vesicle flashes each lasting from 1 to 60 s in duration with anywhere from 0 to 13 flashes in a scene. The results are shown in Table 1, with N_T, N_A, and N_D listed for each scene. The input parameters used were a brightness threshold of 40 (intermediate), the FIR kernel with 16 nonzero elements (large), and a frame skip of 0. The scenes were also tested with other settings. The algorithm did not miss flashes for the seven scenes containing flashes and was unaffected by threshold and kernel size. The algorithm did identify events that were not flashes, however. These were vesicle images that changed size because of fast, oscillatory movements along the plane of the membrane or to movement out-of-focus, but not from dye release. This low specificity was not improved by changing the threshold or kernel size. The number of skipped frames did affect the accuracy and specificity.

Performance was not affected by the brightness threshold because the vesicle flashes were bright. Vesicles ranged in diameter from 2 to 10 μm. The rapid diffusion

TABLE 1 **Vesicle flashes detected**

Scene number	Duration	N_T	N_D	N_A
	in frames			
1	30	0	25	0
2	38	0	27	0
3	120	0	11	0
4	498	0	30	0
5	60	1	2	1
6	260	2	8	2
7	867	5	13	5
8	530	5	19	5
9	300	7	7	7
10	1,854	15	37	15
11	1,527	18	23	18

The input settings of the algorithm for each scene run were a brightness threshold of 40 (intermediate), the large (16 nonzero element) FIR kernel, and a frame skip of 0. N_T denotes the total number of true flashes in each scene, N_D is the number of events detected by the algorithm, and N_A is the number of detected events that were true flashes.

of the released aqueous dye with concomitant dequenching of fluorescence ensured that the spatial profiles of the flashes were larger than the initial diameter of the vesicle (Fig. 2 *A*). The intensities of the difference profiles (Fig. 2 *B*) exceeded even the largest threshold (60 brightness units) that was set.

Detection was also insensitive to the size of the FIR kernel used in the second spatial convolution. With the smaller kernel, brightness gradients were sharpened, giving the annular difference profiles well-defined edges. The larger kernel tended to smooth the profile, but the intensities of the flashes were large enough to compensate for this filtering effect.

The frame skip was the only parameter that affected vesicle flash detection. Flashes were accurately detected with the 0 frame skip (subtraction of a frame from the next consecutive frame). The brightness distribution changed sufficiently within 33 ms to leave a large and bright difference profile (Fig. 2 *B*). With skips of one or two frames, small flashes (arising from 2 μm diameter vesicles) could be missed. Their durations were too short and their peak brightnesses in the difference image were below the streak threshold, or they were initiated within the omitted frame(s). These missed flashes could sometimes be detected by setting the detection threshold to the lowest value or by starting the scene one or two frames later. They were always detected with the 0 skip.

Detection of virion flashes

Virions vs. vesicles

Accurately detecting R18-labeled virion flashes required more effort in fine-tuning the input parameters. These scenes were richer in texture (Fig. 5) and intrinsically variable due to the inhomogeneity of the virus preparations, and the flashes originated de novo from a noisy background after delivery of labeled virus (Fig. 5). The flashes appeared rapidly, often within seconds, after delivery of the virus (Niles and Cohen, 1991*b*). They had to be detected against an intrinsically dynamic background of fluorescence noise, diffuse areas resulting from previous flashes, and bright, moving objects. Virion flashes were detected with less accuracy and specificity than vesicle flashes.

Virion flashes were duller than vesicle flashes because the virion envelope contained fewer dye molecules than the internal compartment of a vesicle. The evolution of the profile was slower for a single virion flash (Fig. 6 *A*), because diffusion of the lipophilic probe within the planar membrane was slower than an aqueous probe in water (Niles and Cohen, 1991*a*). The difference profiles were less intense and more severely degraded by noise than the vesicle profiles, to the extent of being punctated (Fig. 6 *B*). Adjustment of the parameters was crucial for detecting virion flashes.

Cameras

The SIT camera had a low background but yielded dull virion flashes. The greater sensitivity of the intensified CCD camera was obtained at the expense of a high background due to intensifier noise and the amplified fluorescence of the labeled virus and the released lipophilic dye. In Table 2 we show the performance of the algorithm for a number of virion flash scenes. N_T, N_A, and N_D are shown together with the input parameter settings used. Greater accuracy and specificity were obtained with the SIT camera despite its luminance-dependent resolution and lesser sensitivity compared with the intensified CCD camera. These properties of the SIT camera produced better definition of the flash profiles and maintained their spatial contiguity. In the intensified CCD image, the perimeters of the profiles were deteriorated by background noise (Fig. 6 *A*). Difference profiles were punctuated by gaps and were harder for the algorithm to construct into objects. Although the intensified CCD camera detected duller flashes unseen in the SIT camera image, these flashes were less reliably scored by the algorithm. Flash heterogeneity necessitated that different parameters be used for the optimal detection of different flashes. Furthermore, because of the dissimilar sensitivities and signal-to-noise properties of the cameras, neither device could be made to simulate the other. In theory, the SIT camera image could be approximated by an exponentially weighted time series average of the intensified CCD image to compensate for the SIT camera's persistence; however, the different camera properties would require extensive correction of the gain-brightness relation to replicate the true image.

Longer frame skip

Because flash detection relied on determining the change in the spatial brightness profile, the frame skip was an influential parameter. Virion flashes were hard to detect with a frame skip of 0, because dye diffusion was slow. The optimal setting was generally a skip of at least one

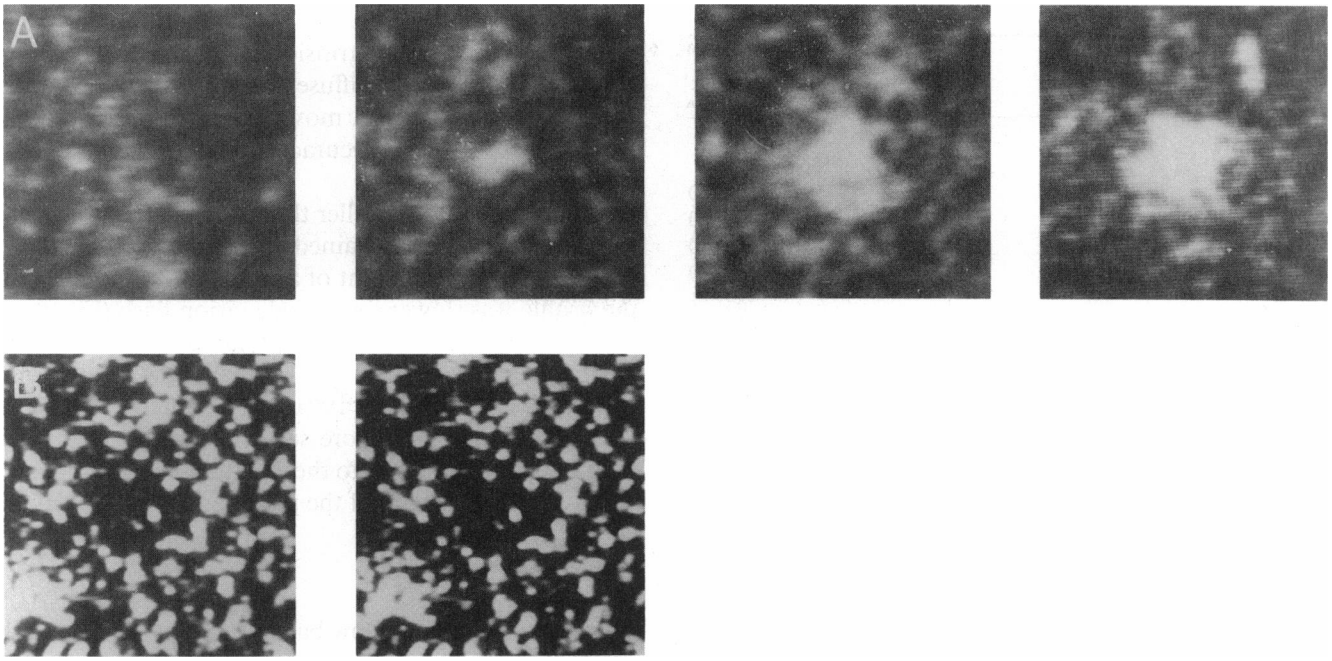

FIGURE 6 A sequence of video frames of a virion flash. (*A*) The first panel shows a region of planar membrane immediately before the eruption of a flash. The second frame shows the same region in the next video frame, which was the first frame of the flash. The third and fourth panels show the fourth and seventh frames in the sequence. The slow diffusion of the released lipophilic dye in the hydrocarbon milieu of the planar membrane produced a slowly evolving video profile with less spatial variegation than the vesicle profiles when displayed as a full interlaced frame. (*B*) The difference profile obtained by subtracting the second from the third panel of *A* (*left*) and the filtered image after the convolutions (as in Fig. 2) with the small kernel (*right*). The virion profile is highly irregular in shape and is almost punctated. To obtain these photographs, intensities were accentuated by maximizing both brightness and contrast of the video monitor and by increasing the exposure time of the film (Technical Pan 135; Eastman Kodak, Rochester, NY). Otherwise, the difference images would be invisible in the photographs. The field width of each panel is 12 μm.

frame. For example, scene 9 (taken with the SIT camera) contained three true flashes. A two-frame skip yielded detection of two of these flashes, a skip of one produced one true flash, whereas a skip of 0 produced no true flashes. The longer skip produced a larger change in the brightness distribution of a flash, which increased accuracy.

Decreased performance with background noise

We examined the effects of the input parameters under worst case conditions by running all combinations on scenes selected for having a noisy background and bright moving objects that oscillated in and out of focus. The results for a scene 15 s in duration containing eight true flashes obtained with the intensified CCD camera are shown in Figs. 7 and 8. The number of events detected (N_D) as a function of brightness threshold and the number of skipped frames are shown in Fig. 7, and the number of accurately detected flashes (N_A) as a function of the same parameters is shown in Fig. 8. In these plots, N_D and N_A are shown for frame delays of 0, 1, and 2, respectively. The moving objects greatly decreased specificity.

In the noisy scene, event detection was most dependent on the brightness threshold. With a frame skip of 0 and the small FIR kernel, the greatest number of events (225) was detected with the intermediate threshold of 40, although only six of the eight true flashes were detected. Fewer events were detected with the largest threshold of 60, but, somewhat surprisingly, no events were detected with the lowest threshold of 20. The background noise in these scenes blended in with the flash profiles and distorted their brightness distributions, making them harder to detect. For all frame delays, the order of the number of true flashes detected was intermediate threshold > highest > lowest. The highest threshold degraded the difference profiles, causing them to fragment into separate objects that were harder to pair with flashes, whereas the lowest threshold included noise in the difference profiles that made them asymmetric.

Accuracy of flash detection in these noisy scenes was less dependent on the frame delay. As shown in Fig. 8, the accuracy for the intermediate threshold was 75% with a frame skip of 0 and was decreased to 63% with skips of one and two. With the longer skips, the brightness profiles were less intense and, hence, degraded by background noise to a greater extent at the longer times causing the flash to be missed. With the highest threshold, the flash profile was isolated from the noise, so that the relatively long duration of the flash profile left spatiotemporally correlated remnants that the algorithm was able to track with the longest skip.

Accuracy was also affected by the FIR kernel size; the greatest number of true flashes was detected with the

TABLE 2 **Virion flashes detected**

Scene number	Duration	N_T	N_D	N_A	Brightness threshold*	FIR kernel size‡	Frame skip§
	in frames						
SIT camera							
1	76	1	3	1	20	16	0
2	47	1	6	1	20	16	2
			7	1	40	16	1
3	215	3	3	2	40	16	1
4	498	13	76	10	40	16	2
5	487	2	5	1	40	8	2
			1	1	20	16	1
			3	2	20	8	2
6	12	0	0	0	20	8	1
7	425	0	0	0	20	8	1
8	71	5	2	0	20	16	2
			4	1	20	8	2
9	160	3	10	2	20	8	2
			6	1	20	8	1
10	89	5	7	5	20	8	2
11	400	4	8	4	20	8	2
			6	0	40	16	1
			11	1	20	16	1
12	400	6	17	6	20	8	2
13	626	9	41	9	20	8	2
Intensified CCD camera							
1	450	3	28	2	40	8	2
			7	0	40	16	2
2	84	1	23	1	40	8	2
			9	1	40	16	1
3	641	3	30	2	40	16	2
			107	2	40	8	2
4	90	0	0	0	40	8	2
5	402	7	37	0	40	8	2
			5	5	60	8	2
			20	0	60	16	2
6	502	5	126	3	40	8	0
			67	5	40	8	2
7	680	7	92	6	40	8	2
			66	2	40	16	2
8	438	5	23	3	40	8	2
			78	4	40	8	0
			47	5	40	8	1
			17	5	60	8	1

* 20, 40, or 60.
‡ Eight nonzero elements or 16 nonzero elements.
§ 0, 1, or 2 frames.

smaller kernel (Fig. 8 and Scenes 5 and 7 under intensified CCD in Table 2). Having zero elements in the small kernel tended to isolate the thin annular portion of the flash profile from the surrounding noise, because noise pixels sufficiently far from the annulus were zero-weighted. Furthermore, these noise pixels were decreased in intensity, because they were uncorrelated with their surrounding pixels. The larger kernel contained no zeros and smoothed the flash profile into the noise.

Spurious events and missed flashes

Although the algorithm detected all flashes arising from vesicles, it missed many virion flashes, and it counted many spurious events not corresponding to flashes. Spurious events originated from the combined effects of background fluorescence, camera noise, and moving objects. With noisy images, the specificity of the algorithm was decreased by scoring bright, moving objects as flashes.

A human observer verified all events detected by the algorithm. Even when a large number of spurious events occurred, it was practical and relatively convenient to check by eye whether each item was, in fact, a flash and to remove the incorrectly identified events from the flash list. The list contained the starting frame number, the duration in video frames, and the x- and y-positions of

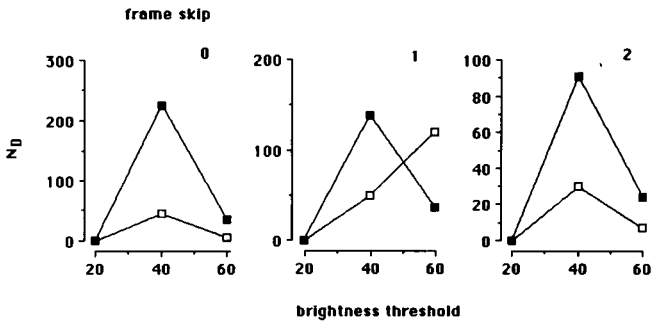

FIGURE 7 Specificity of event detection in a noisy scene for different input parameter settings. The scene lasted 15 s and contained eight virion flashes. The input parameters were set to the values indicated. The number of events detected, N_D, is graphed as a function of brightness threshold for three different frame skips or delays. The left, center, and right panels are for frame skips of zero, one, and two, respectively. In each panel, the open boxes are the results obtained with the large FIR kernel and the closed boxes are for the small kernel.

the centroid of each detected event. A custom flash list editor allowed each identified event to be selected and then displayed in the video frame in which it was first detected so that the human observer was able to make the final decision over whether the event was indeed a flash. Verification also allowed the first frame of the flash to be adjusted with single-frame precision. Each flash was detected at a time that was offset by the frame delay from the time at which it actually began, and this was corrected during verification.

The missed flashes were potentially a more serious problem. Because misses could bias fusion rates, we compared rates of initiation obtained with the algorithm with those measured by a human observer. We determined these rates from the distribution of waiting times (the number of flashes occurring as a function of the time between the ejection of virions and the onset of flashes). Although many steps are involved in viral fusion (binding, pH-dependent conformational changes in the fusion glycoprotein, lipid movements; Skehel et al., 1982) we modeled fusion as a simple two-state, first-order reaction scheme. Although an oversimplified

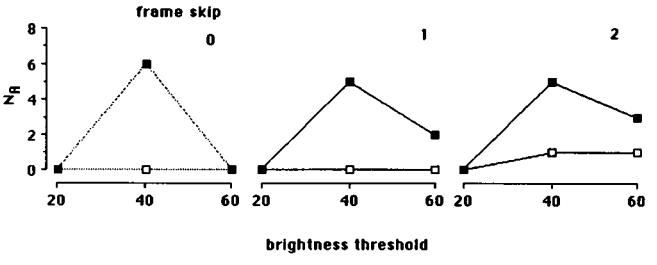

FIGURE 8 Accuracy of flash identification as a function of the input parameter settings for the same scene as in Fig. 7. In each panel (1 for each frame delay), the number of true flashes accurately detected, N_A, is plotted against brightness threshold. Nomenclature is the same as in Fig. 7.

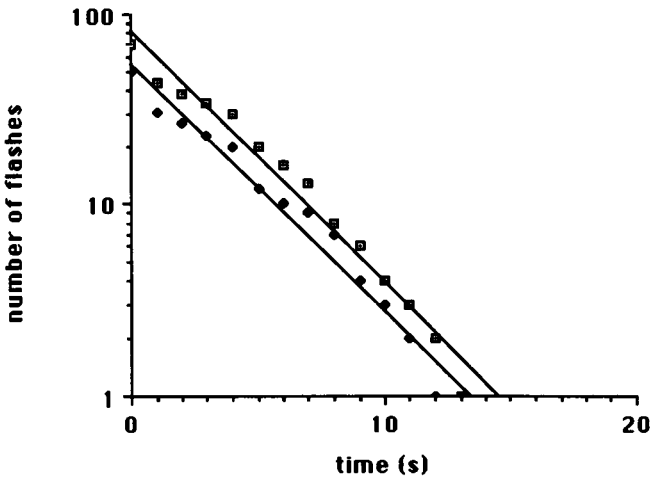

FIGURE 9 Waiting times of virion flash events detected by the algorithm (closed diamonds) and detected by a human observer (open boxes) plotted as log-survivor distributions. R18-labeled influenza virions were ejected at planar membranes composed of asolectin/cholesterol (1:1, by mole fraction) containing 10% gangliosides (GD_{1a} and GT_{1b}) and bathed in a pH 5 buffer solution at 37°C. A total of 7 virion flash scenes were recorded. Each scene began with one or several ejections and then lasted for a period of 5–40 s during which a total of 70 flashes were detected by eye. The algorithm, with settings of a frame skip of two, the small FIR kernel, and a brightness threshold of 40, identified 50 flashes. Flash onset times were measured as described in the text. Waiting time distributions were constructed as log-survivor histograms of the number of flashes with onset times greater than or equal to the indicated time. The exponential rate constants, obtained from least-squares fits, were 0.303 ± 0.015 s^{-1} (slope ± sem) for the flashes detected by eye and 0.295 ± 0.016 s^{-1} for those detected by the algorithm. R^2 was 0.97 for both distributions.

model (Niles and Cohen, 1991*a*, *b*), we were able to check the effect of flashes missed by the algorithm on measured rates of fusion.

We obtained the distribution of waiting times from seven scenes of flashes. The planar membranes contained gangliosides, serving as receptors for the influenza virions (Niles and Cohen, 1991*b*), and were bathed by solutions at acidic pH and 37°C to promote fusion (White et al., 1983). Each scene began with the first ejection of virus at the planar membrane and ranged from 1 to 40 s in duration. To time the flashes by eye, a time stamp superimposed on the video signal in the lower left corner of each frame was used (cf. Fig. 5). For each scene, the time of ejection was marked by when the fluorescent material reached the planar membrane, and the time at which each flash in the scene first appeared was noted. The difference between these two times yielded the time of flash initiation. We accumulated these initiation times (of all flashes in the 7 scenes) into a waiting time distribution and calculated the exponential rate constant as the slope of the line fitted to the log-survivor distribution shown in Fig. 9.

The same scenes were then run one at a time with the algorithm at settings of a frame skip of two, the small FIR kernel, and a brightness threshold of 40. The spuri-

ous events in the flash list generated for each scene were eliminated, and the starting frame number for each true flash was corrected. The time of initiation was then calculated as the difference between the starting frame number of each flash and the number of the first frame of the scene. Because each scene began at a frame obtained during the ejection of virus, these flash times were referred to the first frame of the scene without fine-tuning for the arrival of virus at the planar membrane. After these flash times were sorted as waiting times, the rate constant was calculated from the exponential time constant of the distribution. The algorithm detected 50 out of the 70 true flashes in the scenes. The rate constant measured by eye was within the error of the rate constant measured by the machine (Fig. 9). Therefore, the flashes missed by the algorithm did not affect our measure of the flash rate based on this model.

Improvements

The easiest way to improve the accuracy of the algorithm would be to relax the symmetry moment and brightness distribution criteria. But this would decrease specificity, because more asymmetric difference profiles would be detected. Specificity could be restored by grouping multiple asymmetric objects in a current difference image with each flash identified in the previous difference image. This would allow the algorithm to track a difference profile long after most of its portions had decreased below the streak detection threshold. But this more extensive spatiotemporal correlation would, in turn, be a more stringent criterion and could also decrease accuracy. Better ways would include the use of variable frame delays in a scene, so that both rapidly and slowly changing brightness profiles could be detected. But this would require a more complicated identification procedure to discriminate flashes from moving objects, for example, a variable distance criterion or the higher order moments of the spatial distributions (Jolion and Rosenfeld, 1989). As oscillating and defocusing objects are often encountered as spurious events, a better tracking scheme is desirable with variable termination criteria for the temporally changing objects, such as is used in tracking three-dimensional objects (Iu and Won, 1991).

The most critical part of flash detection is determining the changes in the spatial profile of the diffusing dye. This requires processing the dynamic image by filtering and thresholding operations that alter the brightness distribution. The information about the concentration quenching of the dye and its diffusion that is lost can be recovered by tagging the frame numbers of the start of each flash using the original, unprocessed image. In addition to detecting flashes and measuring fusion rates, the algorithm will be useful in obtaining information about the diffusion and dequenching of the liberated fluorescent dye.

This work was supported by National Institutes of Health grant GM-27367.

Received for publication 22 January 1992 and in final form 24 April 1992.

REFERENCES

Ballard, D. H., and C. M. Brown. 1982. Computer Vision. Prentice-Hall Inc., Englewood Cliffs, New Jersey. 360–362.

Castleman, K. R. 1979. Digital Image Processing. Prentice-Hall Inc., Englewood Cliffs, New Jersey. 106, 327.

Chen, Y.-d., and R. Blumenthal. 1989. On the use of self-quenching fluorophores in the study of membrane fusion kinetics. *Biophys. Chem.* 34:283–292.

Cohen, F. S., J. Zimmerberg, and A. Finkelstein. 1980. Fusion of phospholipid vesicles with planar phospholipid bilayer membranes. II. Incorporation of a vesicular membrane marker into the planar membrane. *J. Gen. Physiol.* 75:251–270.

Frye, L. D., and M. Edidin. 1970. The rapid intermixing of cell surface antigens after formation of mouse-human heterokaryons. *J. Cell Sci.* 7:319–335.

Georgiou, G. N., I. E. G. Morrison, and R. J. Cherry. 1989. Digital fluorescence imaging of fusion of influenza virus with erythrocytes. *FEBS (Fed. Eur. Biochem. Soc.) Lett.* 250:487–492.

Huang, S. K., and S. W. Hui. 1990. Fluorescence measurements of fusion between human erythrocytes induced by poly(ethylene glycol). *Biophys. J.* 58:1109–1117.

Huang, S. K., M. Cheng, and S. W. Hui. 1990. Effect of lateral mobility of fluorescent probes in lipid mixing assays of cell fusion. *Biophys. J.* 58:1119–1126.

Illingworth, J., and J. Kittler. 1988. A survey of the Hough transform. *Comput. Vision Graph. Image Process.* 44:87–116.

Inoue, S. 1986. Video Microscopy. Plenum Press, New York.

Iu, S.-L., and K. Wohn. 1991. Recovery of 3D motion of a single particle. *Pattern Recogn.* 24:241–252.

Jolion, J.-M., and A. Rosenfeld. 1989. Cluster detection in background noise. *Pattern Recogn.* 22:603–607.

Kimme, C., D. Ballard, and J. Sklansky. 1975. Finding circles by an array of accumulators. *Commun. Assoc. Comput. Machin.* 18:120–122.

Lenz, R. 1989. Group-theoretical model of feature extraction. *J. Opt. Soc. Am. A.* 6:827–834.

Lowy, R. J., D. P. Sarkar, Y. Chen, and R. Blumenthal. 1990. Observation of single influenza virus-cell fusion and measurement by fluorescence video microscopy. *Proc. Natl. Acad. Sci. USA.* 87:1850–1854.

Martin, W. N., and J. K. Aggarwal. 1979. Computer analysis of dynamic scenes containing curvilinear figures. *Pattern Recogn.* 2:169–178.

Niles, W. D., and F. S. Cohen. 1987. Video fluorescence microscopy studies of phospholipid vesicle fusion with a planar phospholipid membrane. *J. Gen. Physiol.* 90:703–735.

Niles, W. D., and F. S. Cohen. 1991*a*. Fusion of influenza virions with a planar lipid membrane detected by video fluorescence micrscopy. *J. Gen. Physiol.* 97:1101–1119.

Niles, W. D., and F. S. Cohen. 1991*b*. The role of N-acetylneuraminic (sialic) acid in the pH dependence of influenza virion fusion with planar phospholipid membranes. *J. Gen. Physiol.* 97:1121–1140.

Perin, M. S., and R. C. MacDonald. 1989. Interaction of liposomes with planar bilayer membranes. *J. Membr. Biol.* 109:221–232.

Rubin, R. J., and Y.-d. Chen. 1990. Diffusion and redistribution of lipid-like molecules between membranes in virus-cell and cell-cell fusion systems. *Biophys. J.* 58:1157–1167.

Sarkar, D. P., S. J. Morris, O. Eidelman, J. Zimmerberg, and R. Blumenthal. 1989. Initial stages of influenza hemagglutinin-induced cell fusion monitored simultaneously by two fluorescent events: cytoplasmic continuity and lipid mixing. *J. Cell Biol.* 109:113–122.

Skehel, J. J., P. M. Bailey, E. B. Brown, S. R. Martin, M. D. Waterfield, J. M. White, I. A. Wilson, and D. C. Wiley. 1982. Changes in the conformation of influenza virus hemagglutinin at the pH optimum of virus-mediated membrane fusion. *Proc. Natl. Acad. Sci. USA.* 79:968–972.

Toussaint, G. T. 1980. The relative neighborhood graph of a finite planar set. *Pattern Recogn.* 12:261–268.

White, J., M. Kielian, and A. Helenius. 1983. Membrane fusion proteins of enveloped animal viruses. *Q. Rev. Biophys.* 16:151–195.

Woodbury, D. J. 1986. Fusion of vesicles with planar bilayers: membrane fusion and content release. Ph.D. thesis. University of California, Irvine, CA. 120–160.

Woodbury, D. J., and J. E. Hall. 1988. Role of channels in the fusion of vesicles with a planar bilayer. *Biophys. J.* 54:1053–1063.

Yalamanchili, S., W. N. Martin, and J. K. Aggarwal. 1982. Extraction of moving object descriptions via differencing. *Comput. Graphics Image Process.* 18:188–201.

Zimmerberg, J., F. S. Cohen, and A. Finkelstein. 1980. Fusion of phospholipid vesicles with planar phospholipid bilayer membranes. I. Discharge of vesicular contents across the planar membrane. *J. Gen. Physiol.* 75:241–250.